Int. J. Mach. Tools Manufact. Vol. 28, No. 4, pp.325–339, 1988.
Printed in Great Britain

0890-6955/88$3.00 + .00
Pergamon Press plc

DEVELOPMENT OF A SIX DEGREE-OF-FREEDOM POSITION AND ORIENTATION SENSING DEVICE: DESIGN THEORY AND TESTING

ALEXANDER H. SLOCUM*, DAVID E. HARDT† and LEWIS GREENSPAN‡

(*Received* 17 *March* 1987; *in final form* 28 *August* 1987)

Abstract—This paper focuses on methods of increasing the accuracy of sensor systems for servo controlled articulated structures. Various state-of-the-art motion measuring methods were reviewed and none were found to be entirely suitable for use with articulated structures. Accordingly, a six degree-of-freedom motion measuring system was developed that relied directly (only) on the stability and accuracy of non-contact displacement measuring sensors. A model was tested on a one degree-of-freedom structure and the measured errors were predicted by the error analysis. On the model tested, which had the same error amplification factor as a robot with a 2.3m (90 in.) reach, the one sigma endpoint error was on the order of 13 μm (520 μin.).

1. INTRODUCTION

LARGE industrial robots are inaccurate because they do not have sensors to detect motions other than those of the principal degrees-of-freedom of the joints. To increase accuracy, calibration or end point measurement should be considered.

Machine tool structures (e.g. lathe, milling machine) have been calibrated to compensate for thermal and geometric errors with resultant order-of-magnitude increases in accuracy [1]. For robots, Harjar and Noss [2] developed a method for calibrating a robot by measuring points on a given trajectory and comparing them to programmed points. Dagalakis and Meyers [3] developed a method allowing for repeatable adjustment of gear backlash, so robot programs would not have to be grossly altered after maintenance. Vaishnav and Magrab [4] developed a calibration routine that back-calculates the joint transformation matrices for a robot based on measuring points that the robot was programmed to go to. These methods can help repeatability; however, robots are highly stressed structures, as opposed to machine tools, and considering the number of possible configurations and loads that a robotic structure can be subject to, calibration methods are not easily implemented.

For obtaining end-point feedback of a robot's position, external and internal type sensor systems must be considered. External systems include tracking lasers, millimeter radar, acoustic pingers, and inertial guidance systems. Internal systems include the class of systems broadly known as goniometers.

2. EXISTING SYSTEMS FOR END-POINT POSITION FEEDBACK

A laser tracking system, developed by Lau [5], has the greatest accuracy of any external based system (one part in 100,000), and is based on interferometric and angular mesurement methods. Similar methods have been developed, and are commercially available, that use six laser interferometers triangulating and three cat's eye retroreflectors*. Other optical systems for 3-D tracking have been developed for biomedical applications, but are limited to accuracies of about 12 bits [6–8].

*Center for Systems Automation, Massachusetts Institute of Technology, 77 Massachusetts Avenue, Room 1-143, Cambridge, MA 02139, U.S.A.
†Laboratory for Manufacturing and Productivity, Massachusetts Institute of Technology, 77 Massachusetts Ave., Room 35–234, Cambridge, MA 02139, U.S.A.
‡Automated Production Technology Division, National Bureau of Standards, Gaithersburg, MD 20899, U.S.A.
*Laser interferometer triangulation system available from Chesap Laser Systems Inc., Lanham, MD, U.S.A.

Millimeter radars require large (10"-diameter sphere) antennas [9,10], and are limited in accuracies to 10–12 bits. Acoustic pingers are used mainly in small 2-D and 3-D digitizing machines [11,13] and have accuracies on the order to 10 bits*.

Use of these types of external systems, however, would be difficult to implement unilaterally, because of the potential for the sensing beam to be blocked during some robot motions.

Gyroscopic sensor systems have been considered for robots because they would not have the problem of being obstructed by external objects [14]. The minimum rate sensitivity is governed by the time between updates of actual robot position. With the assumption of update time = 10 min, robot arm length of 1.3m (50 in.), and required accuracy of 25 mm (0.001 in.), the maximum allowable drift rates are about 3.2×10^{-7} rad/sec for rotational sensors, and 1.4×10^{-10} m/s^2 (5.5×10^{-9} in./s^2).

Typical (mechanical) navigational grade gyroscopes (jewelled bearings) can have a sensitivity on the order of 0.008°/h (3.9×10^{-8} rad/s) and high precision gyros (air or magnetic bearings) will have sensitivities on the order of 0.0003°/h (1.5×10^{-9} rad/s) [15]. Fiber optic gyros can detect rotational speeds on the order of 1.0×10^{-6} rad/s [16]. Rates of 4.4×10^{-9} rad/s are predicted [17]; however they are based on the temperature being held to within 0.0067°C [18]. In 1978, a commercial ring laser gyro 0.4 m (17 in.) on a side gave 4.8×10^{-6} rad/s accuracy [19]. Accuracies of 5×10^{-8} rad/s are predicted with the use of mechanical dithering systems to reduce phase lock between the counter propagating beams. For linear motions, a Mach-Zehnder interferometer is capable of sensing accelerations as low as 59 μm/s^2 (0.0023 in./s^2).

In view of the high cost, large size, and limited accuracy of inertial guidance systems for commercial use, it is not likely that they will be used for fixed robotic applications in factory environments in the near future.

Internally-based sensor systems for endpoint feedback can be classified as goniometers. Systems for medical use such as described by Chao [20] or Townsend [21] strap onto an appendage and straddle a joint. Since their mechanical links and joints are not co-linear with the structural members, their sensors must measure rotations and translations in order to obtain accurate measurements. Presently, the devices are limited in accuracy to less than 10 bits.

Examples of goniometric design also exist in manufacturing. The "Spatial Mechanism and Method" patent [22], uses a system of gears and racks to record the three Eulerian angles that a single arm can trace out in space (including twist of the arm about its length) and the extension of the arm via a telescoping tube. Accuracy is on the order of 12–13 bits. The "Monitoring the Location of a Robot Hand" [23] patent describes a knee joint with a planar goniometer attached; however the device does not measure off-axis error components (Abbe errors).

For external measurement, the laser tracking system developed by Lau [5] can provide the necessary accuracy needed for endpoint feedback of robotic manipulators. For cases where environmental conditions limit the applicability of external based systems, an internal based system is needed. No such systems currently exist.

3. GENERAL REQUIREMENTS OF AN INTERNAL BASED SENSOR SYSTEM FOR ENDPOINT FEEDBACK OF ROBOTIC MANIPULATORS

For articulated structures, whose long links greatly amplify angular motions at a joint (Abbe error), all six degrees-of-freedom at each joint will need to be measured. This requires decoupling the sensor and structural systems by using a metrology frame composed of "measuring beams". A measuring beam must be supported so it cannot deform except under the influence of an acceleration on its own mass. For long beams, since the structural beam can deflect sideways in two directions, each end of the measuring beam must be pinned about two orthogonal axes. In addition, since the

* Personal communication with Donald Blomquist, Chief, Automated Production Technology Division, U.S. National Bureau of Standards.

structural beam can twist about its length, one end of the measuring beam must be pinned about an axis parallel to its length. Since the structural beam's length can change, the measuring beam must be held in such a way that one end is free to move along its longitudinal axis.

Possible support schemes for measuring beams include magnetic, air, ball bearings, wire supports, or combinations thereof. Wire support gimbals for limited ranges of motion would be the simplest to design, construct, and maintain. In all cases, the lower the reaction torque and the higher the ratio of the beam moment of inertia to sensor system mass, the lower the induced error in the measuring beam system [24].

The combination of sensors needed at the ends of the measuring beams to provide accurate determination of one large and five small degrees-of-freedom is herein referred to as a POSOR (POSition and ORientation) sensing device. As shown in Fig. 1, one small translational and two small angular degrees-of-freedom can be easily determined by measuring the separation between two essentially parallel plates at three points. Sensors with 12 bit resolution spaced 127 mm (5 in.) will allow for the angles α and β to be determined to 2.4 μrad (0.5 arc-s). The Y distance measurements between the planes, however, provide no information about the relative XZ position or θ rotation of the plates. Two possible systems for detection of these motions are presented here in chonological order: (1) a "Bumpy Ring Sensor" and (2) a "Light Source Ring–Lateral Effect Diode Sensor".

The lateral effect diode system, shown in Fig. 2, consists of a ring of light sources and two lateral effect diodes which provide the XZ coordinates light spots on their surfaces, arranged on the two plates, respectively. The lasers are sequentially pulsed so two light sources do not simultaneously strike the surface of a photo diode. When a pulsed light source beam intersects a diode, its XZ coordinates are measured. The XZ coordinates of two light sources will uniquely define the XZ position and θ rotation of one plane with respect to the other. Angular resolution can be on the order of 1.3 μm/13 cm = 10 μrad.

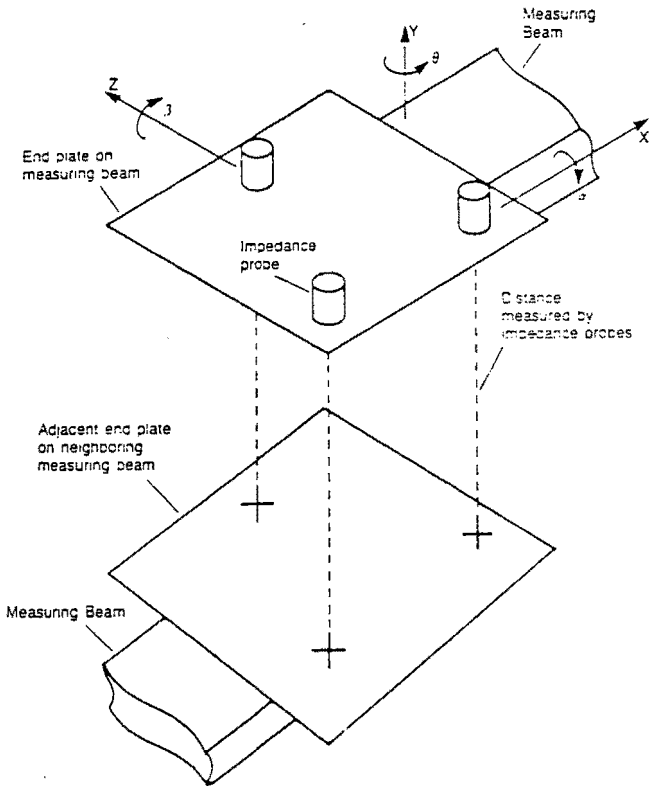

FIG 1. Distance-orientation measurement using distance measuring probes.

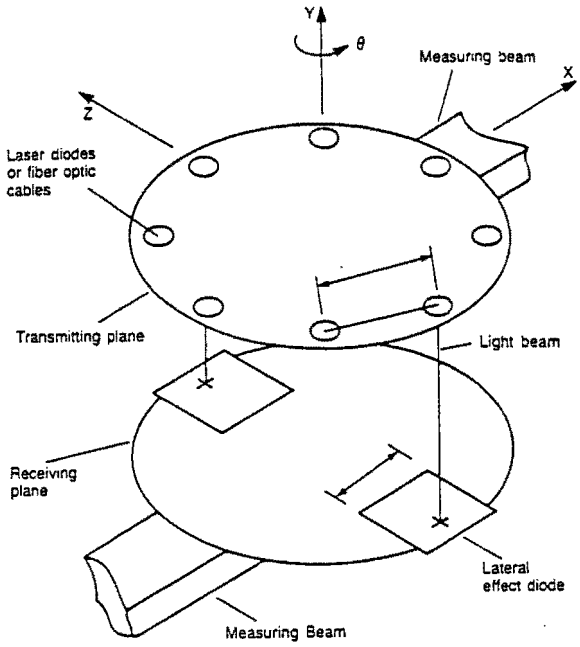

FIG. 2. "Light source-lateral effect diode sensor" for measuring XY position and θ rotation.

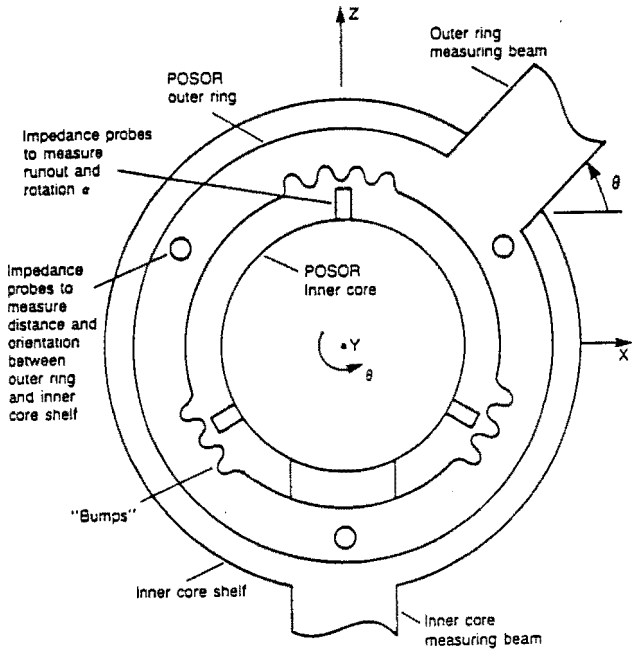

FIG. 3. "Bumpy ring sensor" for measuring XY position and θ rotation.

The Bumpy Ring sensor is shown in Fig. 3. Lateral motion (runout) can be detected with an accuracy of 12 bits by three distance sensors [25] (e.g. capacitance probes). To detect rotation, the sensors are placed out of phase with each other, so that one sensor looks at the peak, one looks at the ramp and one looks at the trough of a bump. The shape of the signals from the three sensors should remain the same as the inner ring undergoes small translations; only the amplitudes should change. Thus by starting from a home bump, runout is determined by looking at the relative amplitude, and rotation is determined by counts and looking at the relative phase of the sensor readings.

For angular sensitivity, if the slant is at 45°, an angular displacement ϵ at a ring radius R_r will produce a sensor reading ϵR_r. If fine bumps are used [1.3 mm (0.05 in.)], an

impedance probe with 0.13 μm (5 μin.) resolution can be used. Thus a measuring device 12.7 cm (5 in.) in diameter could sense rotations of 2 μrad (0.5 arc-s). This system would have to be initially calibrated to account for mechanical inaccuracies in the shape and position of the bumps.

4. CALIBRATION AND TESTING OF A POSOR SENSOR AND MEASURING BEAM

Chronologically, the decision to test a measuring beam system was made before the bumpy ring sensor was developed. It was also desirable to perform mapping tests of lateral effect diodes for use in another project. Thus a prototype POSOR based on Fig. 3 was designed and tested. Appendix A describes the error budget calculations for the POSOR, and Appendix B describes the calibration of the individual POSOR sensors, and the predictions for sensor performance.

The test system consisted of a measuring beam support structure and a lateral effect diode POSOR device as shown schematically in Figs 4, 5 and 6. The major components were: measuring beam, POSOR, two axis stage, twist stage, dial indicators, and a CNC vertical machining center.

A three axis CNC vertical machining center was used as a coordinate measuring machine. The light source plate for the POSOR was used as the stationary reference axes for the POSOR. The stand which held the target plate was bolted and epoxied to the bed of the machine. The measuring beam was supported at each end by two and four degree-of-freedom ball/air bearing gimbals, respectively.

The gimbals were supported by stages which were used to emulate structural beam deflections and one large degree-of-freedom (in the Z direction). A stage for causing twist (α) was located beneath the two degree-of-freedom gimbal near the POSOR. This stage was moved by a jack screw and its motion simulated the twist of a structural beam and bearing runout (motion α, ΔY, and ΔZ). The four degree-of-freedom gimbal was supported by a two axis stage which moved in the Y and Z directions. These motions simulated out-of-plane bending of a structural beam and the large degree-of-freedom motion about a joint. With this system, six degrees-of-freedom could be imposed on the test system.

The accuracy of the vertical machining center along any axis was 5 μm (0.0002 in.). The accuracy to which the angle α could be determined was 81 μrad. When the twist stage was not moved, α should not have changed by more than the runout in the two degree-of-freedom bearings divided by their spacing. Hence α should have been stable to about 1.3 μm/7.6 cm = 17 μrad. Thus, for the translation tests, α measurements were not made. The angles β and θ were measurable with an accuracy of about 6 μrad (5 μm/0.8 m).

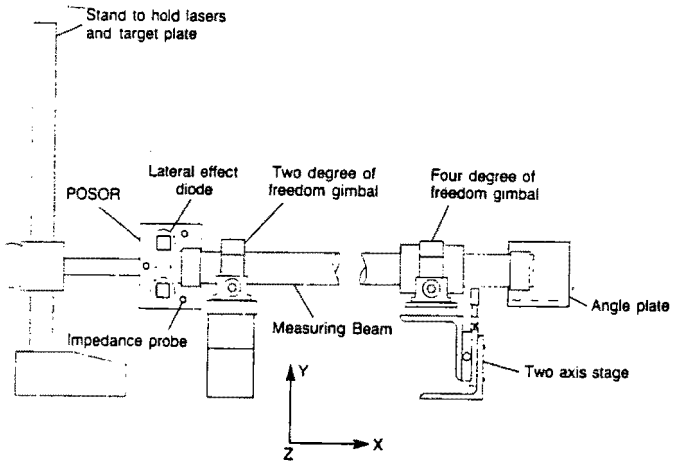

FIG. 4. Schematic of measuring beam POSOR test assembly.

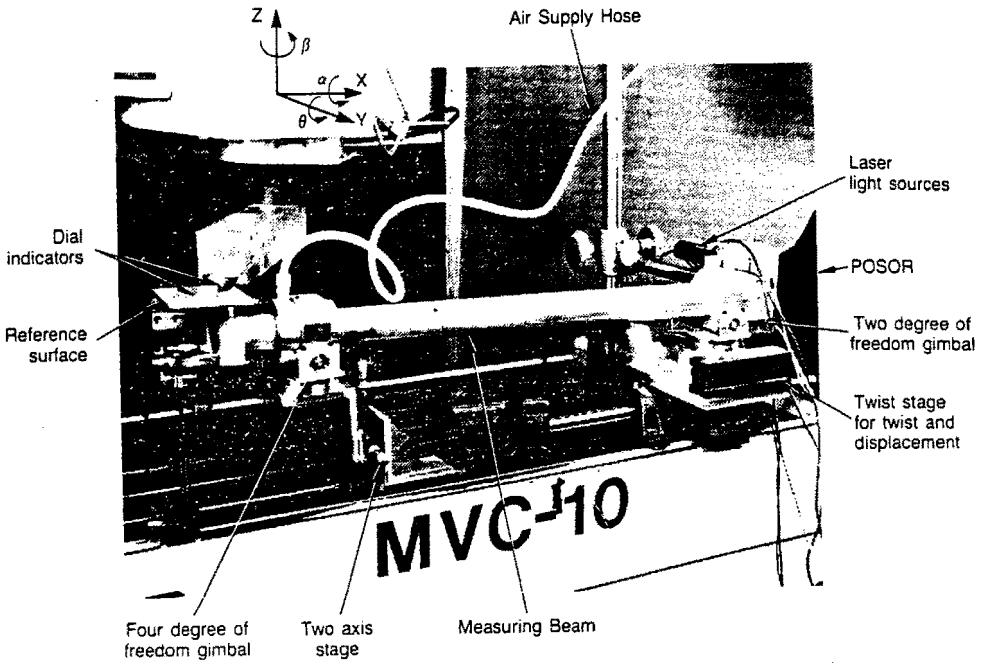

FIG. 5. Test setup for evaluating measuring beam system performance.

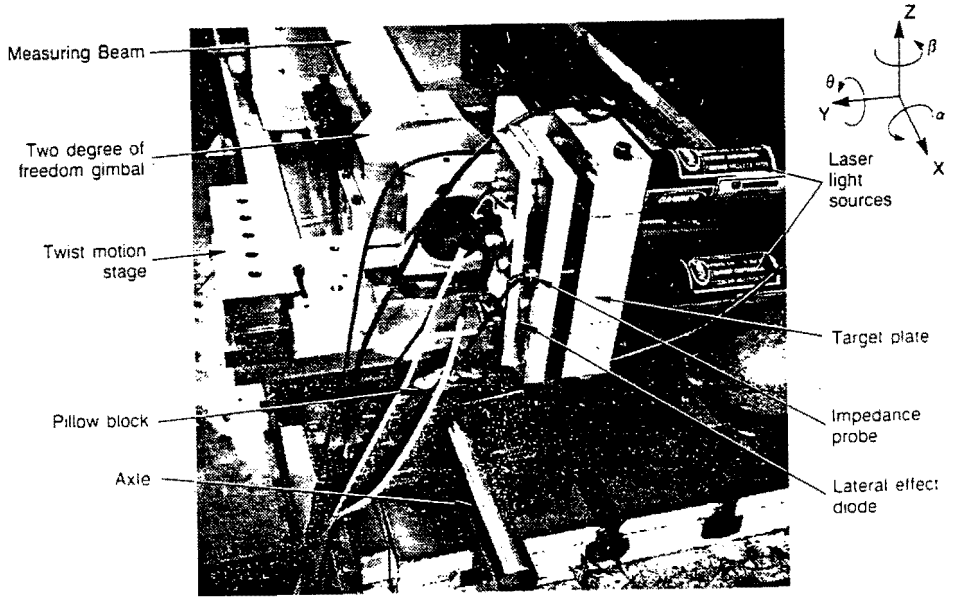

FIG. 6. Measuring beam system's POSOR.

The impedance probes used experienced significant voltage drifts on the order of 0.1 volts over a range of 2 volts. To compensate for this effect, an initial set of calibration measurements was made at the start of each run; however the effect of this voltage drift on the calibration curves derived for the probes was unknown (see Appendix B).

The following tests were performed to evaluate the POSOR performance:

ZMO determined how well the POSOR could measure the angle θ;

YMO determined how well the POSOR could measure the angle β;

YZMO determined how well POSOR could sense motion when more than one degree-of-freedom was moved;

TWIS determined how well the POSOR could measure the angle α and bearing runout;

GEN evaluated POSOR performance when all axes were moved simultaneously.

TABLE 1. SUMMARY OF TEST RESULTS TO EVALUATE MEASURING BEAM SYSTEM PERFORMANCE TEST

		ZMO	YMO	YZMO	TWIS	GEN
Angular motions (μrad)						
	α_{max}	<17	<17	5796	1565
	σ_α	15	3	53	91
Predicted:	$\sigma_{\alpha rand.}$*	11	11	83	83
	$\sigma_{\alpha incr.}$†	<17	<17	<17	<17
	β_{max}	4318	3700	178	217
	σ_β	4	7	49	15
Predicted:	$\sigma_{\beta rand.}$	6	6	6	6
	$\sigma_{\beta incr.}$	13	13	22	5
Linear motions (μm)						
	Y_{max}	3663	3139	151	184
	σ_Y	3	6	41	13
Predicted:	$\sigma_{Y rand.}$	5	5	5	5
	$\sigma_{Y incr.}$	11	11	19	4

*Random error component.
†Decreasing error component, due to error in assumed geometry of sensor placement.

5. TEST RESULTS, RECOMMENDATIONS, AND CONCLUSIONS

Table 1 lists the observed and the predicted errors for the tests. The POSOR measured the angles α and β quite well except for the β motion during the TWIS test.

The θ measurements, which were measured by the lateral effect diode system, were poor and the cause was traceable to the calibration stage for the lateral effect diodes whose errors ended up being mapped onto the diode (see Appendix B). All the tests produced errors that were within three standard deviations of those predicted. Based on these results, the methodology of the error analysis appears correct, and the POSOR's performance for the multi degree-of-freedom tests was similar to that of the single degree-of-freedom tests. This indicates that there is little unidentifiable coupling between the measured degress-of-freedom.

In view of the above, the following recommendations are made concerning future development of POSOR devices.

(1) For impedance probe based devices.

(a) The oscillator demodulator unit must be replaced with a more stable unit. It is suggested that hybrid circuits be used.

(b) The relative probe positions must be found while the angles α and β are simultaneously measured with angular interferometers (see Appendices A and B).

(c) The probes should be secured in a stress free way (gently clamped and epoxied, instead of being held by a threaded housing with locknut).

(2) For lateral effect diode based systems.

(a) Lateral-effect diode-based systems are suitable for use only in laboratory environments because the diodes are very susceptible to contamination.

(b) Plane mirror interferometers should be used to calibrate the diodes.

(c) Stable laser light must be used.

(3) In view of the above problems and complexities, it is recommended that the Bumpy Ring POSOR be investigated in greater detail.

In conclusion note that the average endpoint error measured by the impedance probe system was 16 μm (0.000625 in.), and that of the lateral effect diode system was 0.226 mm (0.008929 in.). Consider that the measuring beam was 0.762 m (30 in.) long and the POSOR was only 0.0762 m (3 in.) in diameter. Thus even if scaled up to a robot with a 1.93m (76 in.) reach as shown conceptually in Fig. 7, the system could provide good endpoint sensor feedback data [24].

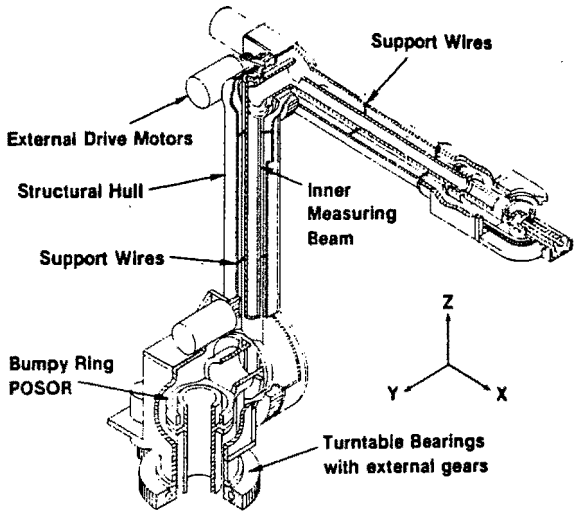

FIG. 7. Conceptual design of a five degree-of-freedom, high payload, high accuracy robot (impedence probes not shown here for clarity.

REFERENCES

[1] T. CHARLETON, *Machine Tool Accuracy Enhancement*, National Bureau of Standards internal document (1979).
[2] M. J. HARJAR and J. S. NOSS, *U.S. Patent #4,372,721*, Feb. 1983.
[3] N. C. DAGALAKIS and D. R. MEYERS, *Int. J. Robot. Res.* **4**, 65–79 (1985).
[4] VAISHNAV and MAGRAB, *Int. J. Robot. Res.* **6**, 59–74 (1987).
[5] K. LAU, R. HOCKEN and W. HAIGHT, paper presented in the *International Conference of Precision Engineering*, Interlaken, Switzerland, 12–17 May 1985.
[6] F. C. CONATI, MSME Thesis, MIT, Cambridge, MA 1977.
[7] J. H. DE VRIES, *Medical and Biological Engineering and Computing*, pp. 213–219, (1980).
[8] E. K. ANTONSSON, Ph.D. Thesis, Dept. M. E., MIT, June 1982.
[9] S. L. JOHNSTON, *Proc. Int. Conf Radar*, Paris, France, pp. 148–159, (1978).
[10] V. J. FALCONE and L. W. ABREU, *IEEE EASCON 1979 Conference Rec.*, pp. 36–41 (1979).
[11] T. UCHIYAMA, S. SEKING and K. TANI, *U.S. Patent #3,924,450*, Dec. 1975.
[12] W. E. HUNT, *U.S. Patent #3,731,273*, May 1973.
[13] J. A. HOWELLS and S. J. SINDEBAND, *U.S. Patent #4,357,672*, Nov. 1982.
[14] A. WECKENMANN and C. LINHART, *Tech. Mess. TM* (Germany) **51**, 165–170 (1984).
[15] M. M. KURITSKY, M. S. GOLDSTEIN, *Proc. IEEE* **71**, 1156–1176 (1983).
[16] K. H. WANSER, R. E. WAGONER, *Photonics Spectra*, 61–66 (1983).
[17] S. LIN, T. G. GIALLORENZI, *Appl. Opt.* **18**, 915–931 (1979).
[18] D. M. SHUPE, *Appl. Opt.* **19**, 654–655 (1980).
[19] H. J. ENGEBRETSON, *Proc. SPIE* **157**, 34–40 (1978).
[20] E. Y. S. CHAO, *J. Biomech.* **13**, 989–1066 (1979).
[21] M. A. TOWNSEND, M. IZAK, R. W. JACKSON, *Biomech.* **10**, 183–193 (1900).
[22] S. E. ROSE, *U.S. Patent #4,419,041*, Dec. 1983.
[23] J. P. W. FLEMMING, *U.S. Patent #4,119,212*, Oct. 1978.
[24] A. H. SLOCUM, Sensor System Design to Determine Position and Orientation of Articulated Structures (Chapter 9), Ph.D. Thesis, MIT, Massachusetts (1985).
[25] D. WHITEHOUSE, *J. Phys. E: Sci. Instrum.* **9**, 531–536 (1976).

APPENDIX A. FORMULATION OF THE POSOR'S ERROR BUDGET

Introduction

Assume that a degree-of-freedom ξ is determined by a function that relates the system geometry and the sensor output. A deviation σ_ζ in each degree-of-freedom ζ that describes the sensors location must be introduced to determine the error σ_ξ produced in the desired measurement:

$$\sigma_\xi = f(\zeta) - f(\zeta + \sigma_\zeta). \tag{A.1}$$

Error budget for the impedance probe system

The general system equations describing the degrees-of-freedom λ_{XY} (distance between the planes at any point X, Y), α, and β (yaw and pitch) assume rotations of the target plane ($X'Y'$ plane) about the X and

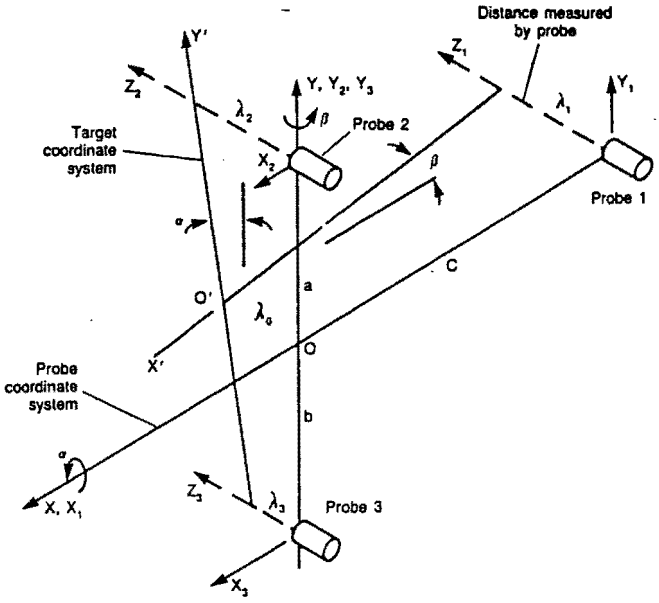

FIG. A.1. Sensor resolution error body diagram for triad of distance measuring sensors.

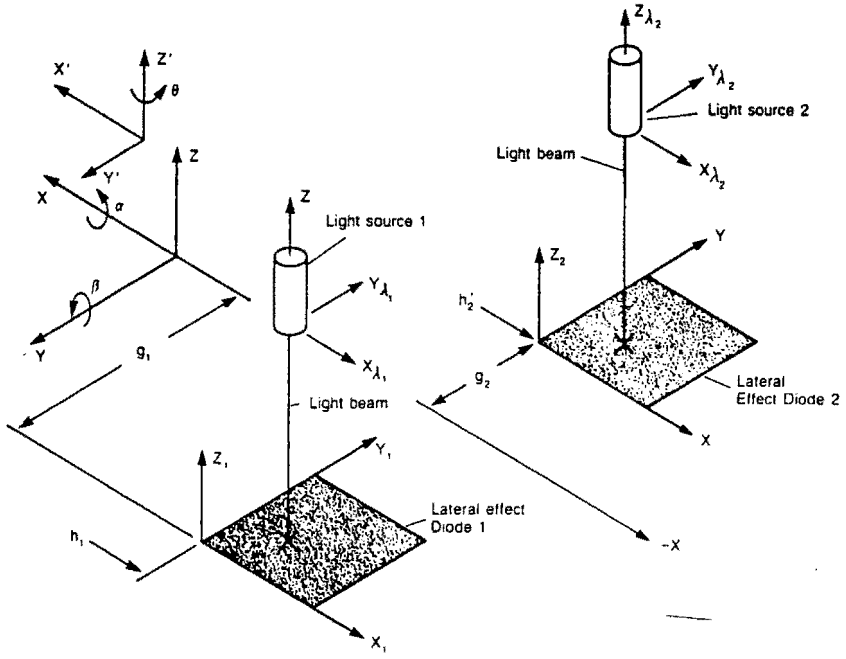

FIG. A.2. Sensor resolution error body diagram for light source lateral effect diode system.

Y axes, respectively, in the sensor coordinate plane, as shown in Fig. A.1:

$$\lambda_{XY} = \lambda_3 + (b + Y)\sin\alpha - X\sin\beta \tag{A.2}$$

$$\alpha = \tan^{-1}(\lambda_2 - \lambda_3/a+b) \tag{A.3}$$

$$\beta = \tan^{-1}\left(\frac{\lambda_1 - (\lambda_2 b + \lambda_3 a)\cdot(a+b)}{c}\right). \tag{A.4}$$

Assuming small angle approximations are valid (A.3) and (A.4) are substituted into (A.2) yield:

$$\lambda_{XY} = \frac{-X\lambda_1}{c} + \frac{\lambda_2}{a+b}\left(b + Y + \frac{Xb}{c}\right) + \lambda_3\left(1 - \frac{b+Y-Xa/c}{a+b}\right). \tag{A.5}$$

273 *Effect of errors in probe readings*

To determine the possible error in the calculation of the distance between planes at any point, $\sigma_{\lambda XY\lambda}$, due to an error $\sigma_{\lambda i}$ in probe #i's reading, λ_i and $\sigma_{\lambda i}$ are inserted into (A.1) with $f(\zeta)$ given by (A.5):

$$\sigma_{\lambda XY\lambda 1} = -\sigma_{\lambda 1} X/c \tag{A.6}$$

$$\sigma_{\lambda XY\lambda 2} = \frac{b + Y + Xb/c}{a + b}\,\sigma_{\lambda 2} \tag{A.7}$$

$$\sigma_{\lambda XY\lambda 3} = \left(1 - \frac{b + Y - Xa/c}{a + b}\right)\sigma_{\lambda}. \tag{A.8}$$

Assuming that $\sigma_{\lambda 1} = \sigma_{\lambda 2} + \sigma_{\lambda 3}$, the root mean square error is:

$$\sigma_{\lambda XY\lambda} = \sigma_{\lambda}\left(\frac{X^2}{C^2} + \frac{(b+Y+Xb/c^2}{(a+b)^2} + \left[1 - \frac{(b+y-xa/c)}{(a+b)}\right]^2\right). \tag{A.9}$$

The angular error $\sigma_{\alpha\lambda i}$ due to an error in the probe reading $\sigma_{\lambda i}$ is determined by applying the principle of equation A.1 to the linearized equation with the following results:

$$\sigma_{\alpha\lambda 2} = \frac{\sigma_{\lambda 2}}{a+b} \tag{A.10}$$

$$\sigma_{\alpha\lambda 3} = \frac{-\sigma_{\lambda 3}}{a+b}. \tag{A.11}$$

Assuming that all the probe errors σ_{λ} are equal yields a root mean square error $\sigma_{\alpha\lambda}$ of:

$$\sigma_{\alpha\lambda} = \sigma_{\lambda}\sqrt{2}/(a+b). \tag{A.12}$$

Similarly, the angular error σ_{β} is:

$$\sigma_{\beta\lambda 1} = \frac{\sigma_{\lambda 1}}{c} \tag{A.13}$$

$$\sigma_{\beta\lambda 2} = \frac{-\sigma_{\lambda 2} b}{c(a+b)} \tag{A.14}$$

$$\sigma_{\beta\lambda 3} = \frac{-\sigma_{\lambda 3} a}{c(a+b)} \tag{A.15}$$

Assuming that all the probe errors σ_{λ} are equal yields a root mean square error $\alpha_{\alpha\lambda}$ of:

$$\sigma_{\beta} = \frac{\sigma_{\lambda}}{c(a+b)}\left[2(a^2 + ab + b^2)\right]^{1/2}. \tag{A.16}$$

Effect of errors in probe spacing

The linear distance between the two plates of the POSOR at any point X, Y is determined by the sensor measurements and the spacing between the sensors as given by (A.5). Inserting a and σ_a into (A.1) with $f(\zeta)$ given by (A.5) gives the following expression for the error $\sigma_{\lambda XY}$ in the calculated distance λ_{XY} between the plates at any λ_{XY} coordinate:

$$\sigma_{\lambda XY a} = \frac{\sigma_a(b+Y+Xb/c)(\lambda_2-\lambda_3)}{(a+b)(a+b+\sigma_a)}. \tag{A.17}$$

Similarly, an error σ_b causes an error $\sigma_{\lambda XYb}$ of:

$$\sigma_{\lambda XYb} = \frac{\sigma_b(Y - a - Xa/c)(\lambda_2-\lambda_3)}{(a + b)(a + b + \sigma_b)} \tag{A.18}$$

and an error σ_c causes an error $\sigma_{\lambda XYc}$ of:

$$\sigma_{\lambda XYc} = \frac{X\sigma_c}{c(c+\sigma_c)}\left(\lambda_1 - \frac{\lambda_2 b + \lambda_3 a}{a + b}\right). \tag{A.19}$$

The last step is to determine the effect on the calculation of the angles α and β from variations in the sensor spacing σ_a, σ_b, and σ_c. Proceeding as before with equation A.1 using (A.3) and then (A.4) for $f(\xi)$.

the following relations are found (assumes $a \gg \sigma_a$ and $b \gg \sigma_b$):

$$\sigma_{\alpha a} \approx \frac{(\lambda_2-\lambda_3)\sigma_a}{(a+b)^2} \tag{A.20}$$

$$\sigma_{\alpha b} \frac{(\lambda_2-\lambda_3)\sigma_b}{(a+b)^2} \tag{A.21}$$

$$\sigma_{\beta a} \approx \frac{(\lambda_3-\lambda_2)b\sigma_a}{c(a+b)^2} \tag{A.22}$$

$$\sigma_{\beta b} \approx \frac{(\lambda_2-\lambda_3)a\sigma_b}{c(a+b)^2} \tag{A.23}$$

$$\sigma_{\beta c} \approx \left(\frac{\lambda_1-(\lambda_2 b+\lambda_3 a)/(a+b)}{c^2}\right)\sigma_c \tag{A.24}$$

With the previous equations, the effect of any system perturbation on the calculated physical quantities λ_{XY}, α, and β can be determined.

Effect of probe misalignment

Since the target plane's rotation is defined by rotations α and β about the X and Y axes, respectively, the equivalent errors in the distance measurement λ_i caused by errors $\sigma_{\epsilon X_i}$ and $\sigma_{\epsilon Y_i}$ are:

$$\sigma_{\lambda_i\alpha} = \frac{\lambda_i\sigma_{\epsilon X_i}(\sigma_{\epsilon X_i}-2\alpha)}{2} \tag{A.25}$$

$$\sigma_{\lambda_i\beta} = \frac{\lambda_i\sigma_{\epsilon Y_i}(\sigma_{\epsilon Y_i}-2\beta)}{2}. \tag{A.26}$$

The total error budget for the impedance probe system of the test POSOR is presented in Table A.1.

Light source-lateral effect diode sensor resolution error budget

Figure A.2 shows the idealized system (the lateral effect diodes' coordinate systems are oriented 180° to the XY coordinate system to match the experimental setup). The $X'Y'Z'$ coordinate system is tilted by the non-Euler angles α and β. The rotation angle θ of the $X'Y'Z'$ coordinate system is defined about the Z' axis. This allows θ to rotate without changing α or β.

In determining the system characteristic equations, the first step is to determine the projected coordinates of the light source onto the lateral effect diode (hereafter referred to as "diode"). Since thge angles α and β are independent, then the offsets associated with the light beam being tilted by α and β will also be independent. The distance $\lambda_{XY\lambda_i}$ from the light spot to the light source plane is found by substituting the light spot coordinates X_{di} and Y_{di} into (A.5). From Fig. A.3, the projected coordinates are found to be:

$$X_{\lambda pi} = h_i - X_{di} + \lambda_{XY\lambda_i}\frac{\cos\alpha\sin2\beta}{2} \tag{A.27}$$

$$Y_{\lambda pi} = g_i - Y_{di} - \lambda_{XY\lambda_i}\frac{\cos\beta\sin2\alpha}{2}. \tag{A.28}$$

To determine the projected coordinates X_0 Y_0 of the $X'Y'Z'$ origin, the projected distances of the light sources' coordinates must be subtracted from (A.27) and (A.28):

$$X_0 = h_i - X_{di} + \lambda_{XY\lambda_i}\frac{\cos\alpha\sin2\beta}{2} - h_{\lambda_i}\cos\beta \tag{A.29}$$

$$Y_0 = g_i - Y_{di} - \lambda_{XY\lambda_i}\frac{\cos\beta\sin2\alpha}{2} - g_{\lambda_i}\cos\alpha. \tag{A.30}$$

The angle θ of rotation of the $X'Y'Z'$ coordinate system about its Z' axis is found from the weighted difference of the Y_{di} and X_{di} coordinates of the light spots. The weighting (by $\cos\alpha$ and $\cos\beta$, respectively) is necessary to prevent a rotation α (or β) from changing one leg of the slope of the triangle. The angle θ is, thus:

$$\theta = \tan^{-1}\left(\frac{(-Y_{d1}+g_1+Y_{d2}-g_2)\cos\alpha}{(-X_{d1}+h_1+X_{d2}-h_2)\cos\beta}\right). \tag{A.31}$$

The error in the $X'Y'Z'$ origin location (ignoring second order effects from calculation of $\lambda_{XY\lambda}$) is directly proportional to the errors in the diode and light source location coordinates, the diode accuracy, and to a

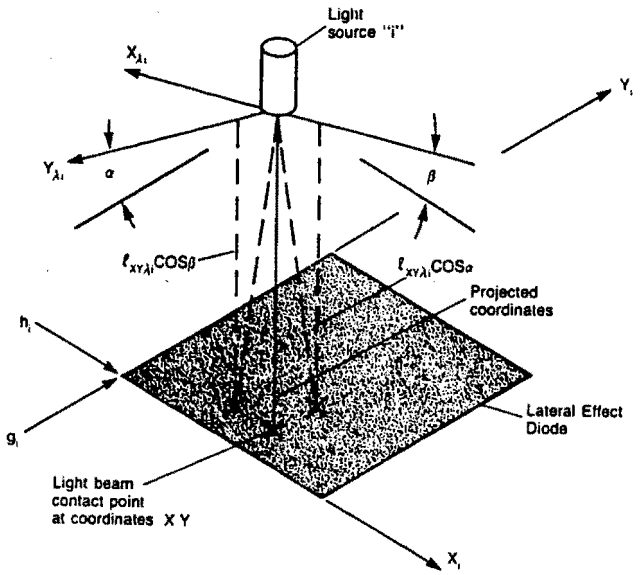

FIG. A.3. Geometry to determine projected coordinates of light source in XYZ coordinate system.

lesser extent the angles α and β, as can be seen from equations A.29.

In order to find the error in the angle θ ($\theta \approx 90° \pm \Delta\zeta$), assume:

$$\cot^{-1}(f(\zeta)) - \cot^{-1}(f(\zeta + \Delta\zeta)) = (f(\zeta)) - (f(\zeta + \Delta\zeta)). \tag{A.32}$$

Thus errors in θ can be calculated using equation A.1 with $f(\zeta)$ given by:

$$f(\zeta) = \frac{(-X_{d1} + h_1 + X_{d2} - h_2)\cos\beta}{(-Y_{d1} + g_1 + Y_{d2} - g_2)\cos\alpha}. \tag{A.33}$$

This assumption will in effect cause a phase shift of 90°, so the σ_X is really the σ_Y and vice versa.

To determine the effect of errors σ_X and σ_Y on X_0, Y_0 and θ equation A.1 is used with $f(\zeta)$ given by equations A.29, and A.33. $\sigma_{x0} = \sigma_x$, and $\sigma_{y0} = \sigma_y$

$$\sigma_{\theta X} = \frac{(-X_{d1} + h_1 + X_{d2} - h_2)\cos\beta}{(-Y_{d1} + g_1 + Y_{d2} - g_2)^2\cos\alpha}\,\sigma_X \tag{A.34}$$

$$\sigma_{\theta Y} = \frac{\cos\beta\,\sigma_Y}{(-Y_{d1} + g_1 + Y_{d2} - g_2)\cos\alpha}. \tag{A.35}$$

TABLE A.1. TOTAL ERROR BUDGET FOR IMPEDANCE PROBE SYSTEM FOR TEST POSOR

Perturbation error	Induced error ($\sigma_{\lambda,0,0}$)*†	Induced error ($\sigma_{\lambda=1.5}$)*†	Induced error (σ_α-in)*‡	Induced error (σ_β-in)*§
Sensor measurement and position errors				
σ_λ	$0.0280\sigma_\lambda$	$0.0307\sigma_\lambda$	$0.0185\sigma_\lambda$	$0.0323\sigma_\lambda$
σ_a	$0.0003\sigma_a$	$0.0005\sigma_a$	$0.0002\sigma_a$	$0.0001\sigma_a$
σ_b	$0.0003\sigma_b$	0.0	$0.0002\sigma_b$	$0.0001\sigma_b$
σ_c	0.0	$0.0001\sigma_c$	0.0	$0.0002\sigma_b$
Sensor orthogonality errors				
$\sigma_{\epsilon X}$	$0.0007\sigma^2_{\epsilon Y}$	$0.0008\sigma^2_{\epsilon X}$	$0.0005\sigma^2_{\epsilon X}$	$0.0004\sigma^2_{\epsilon X}$
$\sigma_{\epsilon Y}$	$0.0007\sigma^2_{\epsilon Y}$	$0.0008\sigma^2_{\epsilon Y}$	$0.0005\sigma^2_{\epsilon Y}$	$0.0004\sigma^2_{\epsilon Y}$

*Assumes $a=b=38.1$ mm, $c = 76.2$ mm
†From equation A.9
‡From equation A.12
§From equation A.16

Light source-lateral effect diode sensor alignment error budget

The effect of X or Y position errors in the light source and diode locations on system error can be obtained from equations A.34 and A.35, respectively. Equivalent translational errors for orientation errors in the light source and diode locations are obtained from the geometry shown in Fig. A.3. The total error budget for the light source-lateral effect diode system is presented in Table A.2.

TABLE A.2. TOTAL ERROR BUDGET FOR LIGHT SOURCE-LATERAL EFFECT DIODE SYSTEM FOR TEST POSOR

Perturbation error	Equivalent diode error $(\sigma_X)^*$	Equivalent diode error $(\sigma_Y)^*$	Induced error in θ†
σ_X			$0.0023\sigma_X$
σ_Y			$0.0131\sigma_Y$
$\sigma_{X\alpha}$‡	0.0	$6.35\sigma^2_{X\alpha}$	
$\sigma_{Y\beta}$‡	$6.35\sigma^2_{Y\beta}$	0.0	
$\sigma_{Z\theta}$§	$6.35\sigma^2_{Z\theta}$	$6.35\sigma^2_{Z\theta}$	
$\sigma_{Z\gamma}$‖	$6.35\sigma^2_{Z\gamma}$	$6.35\sigma^2_{Z\gamma}$	
$\sigma_{X\lambda\alpha}$¶	$1.27\sigma_{X\lambda\alpha}$	0.0	
$\sigma_{Y\lambda\beta}$¶	0.0	$1.27\sigma_{Y\lambda\beta}$	

*Assumes $X_{d1} = Y_{d1} = X_{d2} = Y_{d2} = 12.7$ mm. $\lambda_{XY\lambda} = 1.27$ mm.
†Assumes $X_{d1} = Y_{d1} = Y_{d2} = 0$, $X_{d2} = 12.7$ mm, $h_1 = h_2 = -25.4$ mm, $g_1 = 38.1$ mm, $g_2 = -38.1$ mm. Values for σ_x and σ_y must also be in mm.
‡Parallelism error between diode and XY plane (rad).
§Parallelism error between diode's axes (rad).
‖Non-orthogonality of a diode's axes (rad).
¶Light source orientation errors (rad).

APPENDIX B. METHODS AND RESULTS OF CALIBRATION AND TESTING PROCEDURES OF A MEASURING BEAM SYSTEM FOR ARTICULATED STRUCTURES

Introduction

During the entire experiment, the temperature in the room never varied more than 0.1°F (0.06°C). By keeping the distance between the optics less than 12.7, 50.8, 254 mm (0.5, 2 and 10 in.) for the impedance probes and the lateral effect diode Y and X axis measurements respectively, the thermal growth error due to the cast iron stage would be at most 0.01, 0.03, and 0.15 μm (0.3 μin., 1.2 μin. and 6.0 μin.), respectively. The principal error in the laser interferometer measurements occurred from the changing barometer readings which affect the velocity of light compensation factor. For 24 hr runs, the worst case error was (0.999730 − 0.999735) = 5 μm/m. For any one calibration run (less than 12 hr) the error was (0.999730 − 0.999731) = 1 μm/m. In general, tests were not run when a change in the weather was to be expected. The electronics were not affected by the small variations in air properties as was shown by testing with a standard reference voltage supply.

For the distance measurements made, the alignment of the axes of the laser interferometer, the actuation stage, and the sensor was done using a dial gauge set in the spindle of the vertical machining center. The maximum alignment error was at most 5 μm/25 mm.

For the CNC vertical machining center used as a stage, the angular motions about the X and Y axes were all about 1 arc-s per 25 mm of travel, and the straightness was on the order of 0.13 μm/m of travel.

The straightness, yaw, and pitch of a computer controlled stepper motor driven ball slide stage with 20mm of travel were measured using a laser interferometer. Six runs were made with a mean variation in straightness of 10 μm (0.000408 in.). The repeatability, however was only on the order of 0.0254 mm (0.001 in.). The yaw had a repeatability of about 5 arc-s. The pitch had a repeatability of about 2 arc-s with the exception of a bump of about 10 arc-s at an X position of 7.6 mm (0.3 in.). Unfortunately, these errors were mapped onto the lateral effect diodes; thus this stage proved to be the principal source of error in the experiments.

The net effect of all the errors in the light source-lateral effect diode system are listed in Table B.1. The worst errors were due to the calibration stage and to the error in diode axes X offset. The root mean square of the errors indicates that the Light Source-Lateral Effect Diode system will have errors of:

$\sigma_X = 39$ μm (1572 μin.), $\sigma_Y = 5$ μm (207 μin.), and $\sigma_u = 115$ μrad.

The net effect of all the errors in the impedance probe system are listed in Table B.2. The worst errors were due to the voltage drift in the electronics, and the errors in measuring the probe spacings a, b, and c. Solutions for both of these problems are: stabilize the electronics, and use two angular interferometers.

Two types of error are apparent, the random component and the steadily increasing component. The former is due to the error in the linearization curves (≈ 0.13 μm) and drift in the probe electronics. For probes 1, 2, and 3, these errors are 0.13, 0.5, and 0.63 μm (5, 20, and 24 μin.), respectively. The latter is due to "fixed errors" in the physical parameters of the system, as well as error in determining the zeros voltage drift of the probes. Due to the nature of the error calculations (equation A.1) these latter types of errors will increase from zero to the maximum value as the measured degree-of-freedom increases.

TABLE B.1. RESULTS OF LIGHT SOURCE-LATERAL EFFECT DIODE SYSTEM CALIBRATION

Perturbation error	Value (μm)	Induced σ_X (μm)	Induced σ_Y (μm)
Axes offset errors			
σ_X	39.141	39.141	0
σ_Y	0.939	0	0.889
Linearization errors			
σ_{X1}	5.309	5.301	0
σ_{Y1}	3.480	0	3.479
σ_{X2}	5.232	5.232	0
σ_{Y2}	2.159	0	2.159
Repeatability			
σ_{X1}	2.032	2.032	0
σ_{Y1}	2.032	0	2.032
σ_{X2}	1.270	1.270	0
σ_{Y2}	1.270	0	1.270
Interpolation error			
σ_{X1}	0.889	0.889	0
σ_{Y1}	0.635	0	0.635
σ_{X2}	0.635	0.635	0
σ_{Y2}	0.762	0	0.765
Angular errors (μrad)			
Diode flatness			
$\sigma_{X\alpha 1}$	5000	0	0.160
$\sigma_{Y\beta 1}$	5000	0.160	0
$\sigma_{X\alpha 2}$	5000	0	0.160
$\sigma_{Y\beta 2}$	5000	0.160	0
Diode axes orthogonality error			
$\sigma_{Z\Theta}$	2800	0.051	0.051
$\sigma_{Z1\gamma}$	2800	0.051	0.051
$\sigma_{Z2\gamma}$	2800	0.051	0.051
Light source orientation errors			
$\sigma_{X\lambda 1\alpha}$	514	0·653	0
$\sigma_{Y\lambda 1\beta}$	1045	0	1.328
$\sigma_{X\lambda 2\alpha}$	509	0.647	0
$\sigma_{Y\lambda 2\beta}$	933	0	1.186
Root mean square errors		39.942	5.245
Root mean square error in angle θ: 115μrad			

The root mean square of the errors indicates that the impedance probe system will have angular errors of σ_α = 132 μrad and σ_α = 115 μrad. The errors in calculated distance between the plates at the origin and at a lateral effect diode are $\sigma_{\lambda,0,0}$ = 5 μm (196 μin.) and $\sigma_{\lambda=1.1.5}$ = 5 μm (205 μin.), respectively.

TABLE B.2. RESULTS OF IMPEDANCE PROBE SYSTEM CALIBRATION: TOTAL ERROR BUDGET

Perturbation error	Induced $\sigma_{\lambda 0,0}$ (μm)	Induced $\sigma_{\lambda-1,1,5}$ (μm)	Induced σ_α (μrad)	Induced σ_β (μrad)
Errors that increase with the degree of freedom measured:				
Linear errors				
σ_a = 344 μm	2.87	3	76	38
σ_b = 439 μm	3.63	0	97	48
σ_c = 186 μm	0	0.508	0	41
Probe orientation errors				
$\sigma_{\alpha\beta\lambda i} \rightarrow \sigma_\lambda$ = 0.127 μm	0.102	0.102	2	7
$\sigma_{\epsilon x i} \rightarrow \sigma_\lambda$ = 0.102 μm	0.076	0.076	2	7
$\sigma_{\epsilon y i} \rightarrow \sigma_\lambda$ = 0.102 μm	0.076	0.076	2	7
Voltage supply errors				
$\sigma_{\lambda 1}$ = 0.457 μm	0	0.154	0	6
$\sigma_{\lambda 2}$ = 0.533 μm	0.279	0.432	7	4
$\sigma_{\lambda 3}$ = 0.406 μm	0.203	0.076	5	3
Root mean square values:	4.62	4.80	123	75
Random errors				
$\sigma_{\lambda 1}$ = 0.178 μm	0	0.076	0	3
$\sigma_{\lambda 2}$ = 0.533 μm	0.279	0.432	7	4
$\sigma_{\lambda 3}$ = 0.635 μm	0.330	0.102	8	4
Root mean square values:	0.432	0.457	11	6